Aerospace Heat Exchanger Technology 1993
R.K. Shah and A. Hashemi (Editors)

INVESTIGATION OF LOCAL HEAT TRANSFER IN COMPACT HEAT EXCHANGERS BY HOLOGRAPHIC INTERFEROMETRY

F. Mayinger, J. Klas

Lehrstuhl A für Thermodynamik, TU München, Arcisstraße 21
D – 8000 München 2

1. ABSTRACT

Compact heat exchangers are key components for the development of future aircraft devices. An enhancement of the heat transfer rate results in a decrease of the heat exchanger size and thus in lower weight and lower investment costs. An exact knowledge of the temperature distribution in the boundary layer is necessary for a specific augmentation of heat transfer. For this reason the holographic interferometry was applied as measuring method enabling a visualization of the temperature field without disturbing the flow pattern. The local Nusselt number was determined from the isotherms at the wall. A digital image processing system was used for the evaluation of interferograms. The measuring method is demonstrated for three different types of geometries for compact heat exchangers using air as test fluid:

- Plain fin arrangements of plate-fin heat exchangers
- Flow in a profile shaped duct for tubular matrices
- Flow over circular segment shaped turbulence promotors

During the experiments the Reynolds number was varied between 500 and 3000, a range, where low pressure losses occurred. The test section was heated by hot water in order to obtain a constant wall temperature as thermal boundary condition.

2. INTRODUCTION

An enhancement of the heat transfer rate results in a decrease of the corresponding heat exchanger. Generally the heat transfer rate in a heat exchanger can be calculated by

$$\dot{Q} = \Delta T_m U \beta V, \tag{1}$$

Therefore improvements of heat transfer can be achieved by increasing exchanger volume V, area density β of the exchanger, logarithmic mean temperature difference ΔT_m or

overall conductance U, including the heat transfer coefficients and the conductivity of the wall. The convective heat transfer coefficient of gases usually is one or two orders of magnitude lower than that of liquids. For this reason a high heat transfer area is necessary for realizing a high heat transfer rate, especially if one or more fluids are gaseous. This means the surface must be compact. It is defined, that a heat exchanger is compact, if it incorporates at least one compact surface [1] . Shah specified that a surface is compact, if the area density is greater than 700 m^2/m^3. On the other hand heat exchangers with densities of 6600 m^2/m^3 are also used [2] .

For a specific improvement of heat exchanger surfaces the exact knowledge of the temperature distribution, especially in the boundary layer, is a useful aid. Because of the thin boundary layer it is impossible to apply a direct mechanical measuring gauge. For this reason the holographic interferometry, a combination of holography and interferometry, described by Hauf, Grigull [3,] Mayinger, Chen [4] and Mayinger, Panknin [5] was chosen allowing a continuous visualization of the temperature field without disturbing the flow pattern. Because of the wide acceptance of this method an explanation of this well-known measuring technique is omitted in this paper. But it should be mentioned that the interference lines of the interferograms are identical to the isotherms of the investigated duct flows. From the distance between the isotherms the heat flux and therefore the local Nusselt number distribution can be calculated. Due to digitizing effects and ligth deflections a uncertainty of the measuring technique of less than 10 % was achieved. The accuracy is slightly decreased for laminar flow because of the therefore thicker boundary layer.

3. THE EXPERIMENTAL SET-UP

The description of the experimental set-up for investigating plain fin arrangements and duct flows through the profile shaped duct is facilitated by referring to Fig. 1. The test section was performed in a sandwich construction with the upper part removable enabling an employment of different test matrices with variable height and size. The thermally insolated inlet section leads to a hydrodynamically almost developed air flow, with a thermally developing flow regime in the test matrices. The test section itself is heated by six water-supplied heating plates. The temperature of each plate is measured by thermocouples in order to obtain a uniform wall temperature of the test matrix surface. The laser beam passes the test chamber in the same direction as the fluid flow and leaves it at the exit through an ordinary sheet of glass closing the outlet of the test section. Mass flow rates and thus Reynolds numbers in the test matrix are determined by orifices with a accuracy of 3 %. Air temperatures at the entrance and at the exit of the test matrix are measured by seven thermocouples allowing a calculation of the logarithmic mean temperature difference. Due to measurement uncertainties a accuracy of the global heat balance of less than 10 % is reached. Air flow is produced by a suction pump equipped with a flow regulating throttle. For the examinations of turbulence promotors the test section was modified. In this case the laser beam penetrates the test section perpendicular to the air flow, so that the side walls were performed transparent.

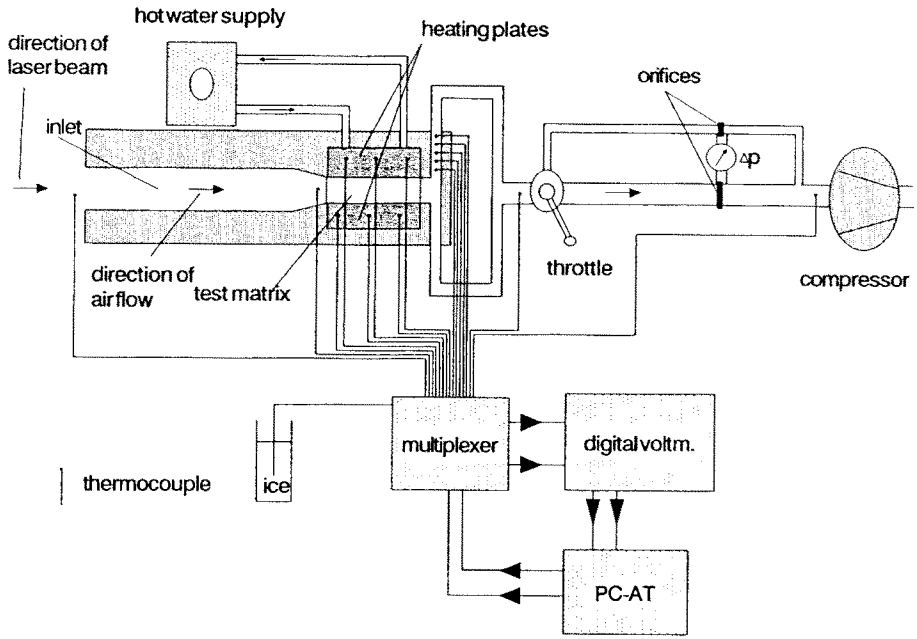

Fig.1 Experimental Setup

A digital image processing system is employed to evaluate the interferograms. The interference patterns are filmed with a CCD-camera and changed into a digital image of 768 ×512 points by a digitizer board fixed to a PC–AT. An interactive control-programme for this system was written in the programming language C. Several possibilities exist in order to improve the quality of the interferograms like digital filters, contrast enhancement and noise reducing procedures. Within this programme the distribution of grey values along lines normal to the surface of the test matrix can be scanned. Local maximum and minimum grey values along these lines are obtained automatically in order to determine the distance between the interference lines and with that local heat transfer coefficients.

4. HEAT TRANSFER IN PLAIN FIN ARRANGEMENTS

During the first phase of our experiments the heat transfer in plain fin arrangements presented in Fig. 2 was investigated. Three test matrices with different corner radii of 1 mm, 3 mm and 5 mm were manufactured. The ducts were milled out of 12 mm thick sheets of aluminum with a fin thickness of 2 mm. The exact dimensions are summarized in Table 1. The hydraulic diameter d_{hyd} of the ducts is calculated by:

$$d_{hyd} = \frac{4A_c l}{A} \tag{1}$$

Table 1 Dimensions of plain fin arrangements

		matrix 1	matrix 2	matrix 3
heigth of fins	e	10 mm	10 mm	10 mm
width of duct	b	10 mm	10 mm	10 mm
length	l_r	300 mm	300 mm	300 mm
fin thickness	t_f	2 mm	2 mm	2 mm
radius	r	1 mm	3 mm	5 mm

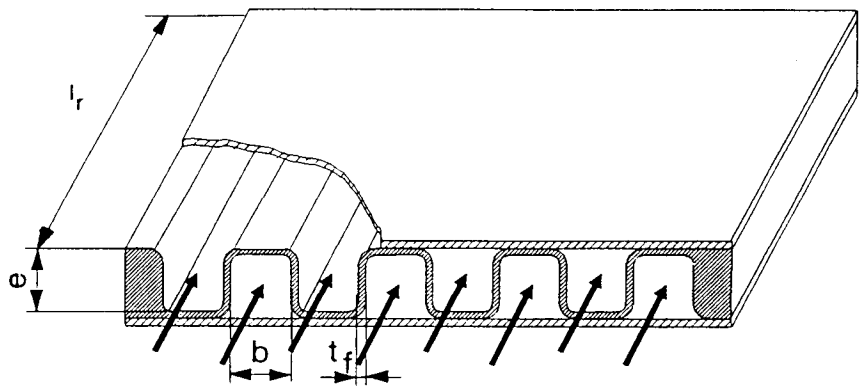

Fig. 2 Plain fin arrangement in compact plate heat exchangers

considering the flow cross-sectional area A_c, the duct length l and the total heat transfer area A.

Two typical interference patterns are presented in Fig. 3 for different corner radii, describing the temperature distribution averaged over the whole test section. Due to the length of the test section the temperature difference between two neighbouring isotherms is approximately 2.3 K. The local distribution of the Nusselt number is shown in Figs. 4 to 6 with Reynolds numbers of 500, 1500 and 2500, respectively. Comparing the figures, one can easily recognize, that the local heat transfer is proportional to the fringe density at the corresponding wall.

For low Reynolds numbers typical laminar flow patterns are established resulting in a maximum heat transfer in the middle between two adjacent corners. On the other hand the heat flux decreases at the corners. It seems that the heat flux vanishes at the convex corners because the flow is stagnant at this area.

For turbulent flow the effect of the convex bent radii as turbulence generators can be recognized, because of the local maxima of the heat flux in the direct neighbourhood of

r = 1mm
Re = 500

r = 5mm
Re = 2500

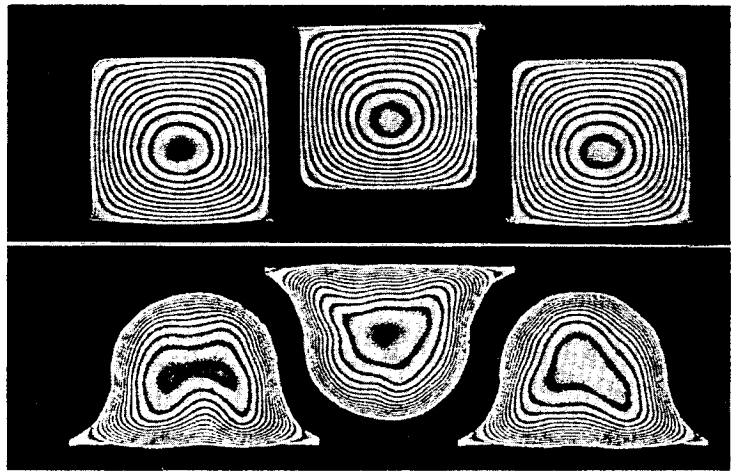

Fig. 3 Interferograms for plain fin arrangements

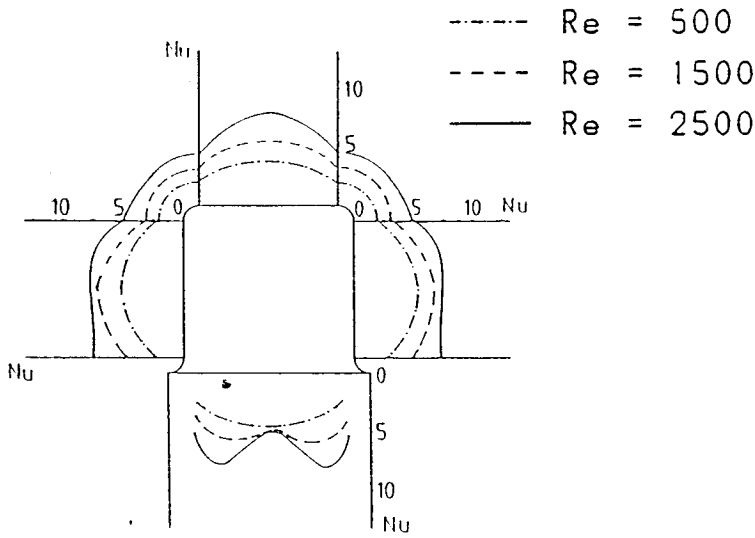

Fig. 4 Local distribution of Nusselt number for square ducts with corner radii of 1 mm

the corners. Contrary to the laminar flow the heat flux decreases only in the immediate vicinity of the convex corners.

Figure 7 shows the average Nusselt numbers calculated from the interferograms and from the energy balance as a function of the Reynolds number. Comparing both Nusselt numbers the high accuracy of the measuring technique is demonstrated by the small difference of less than 7 % between the overall heat balance and the interferometric measurements.

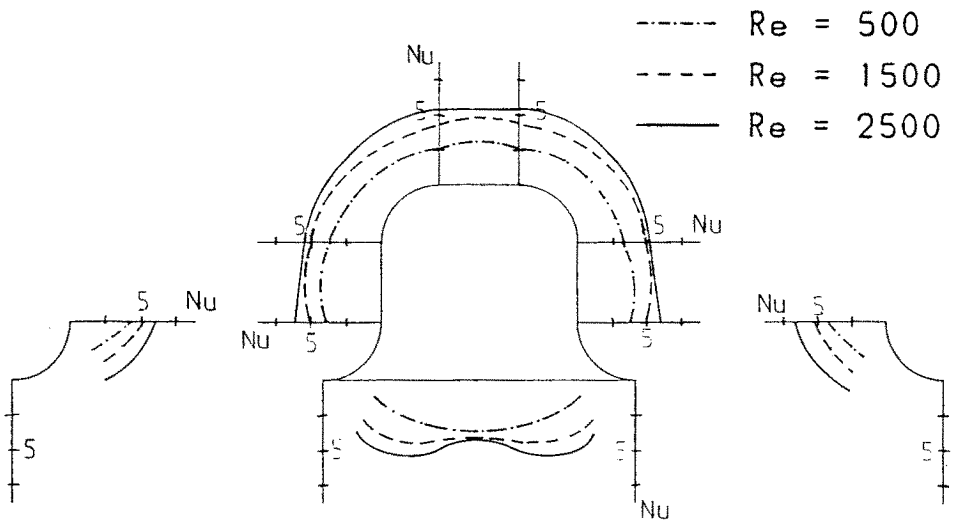

Fig. 5 Local distribution of Nusselt number for square ducts with corner radii of 3 mm

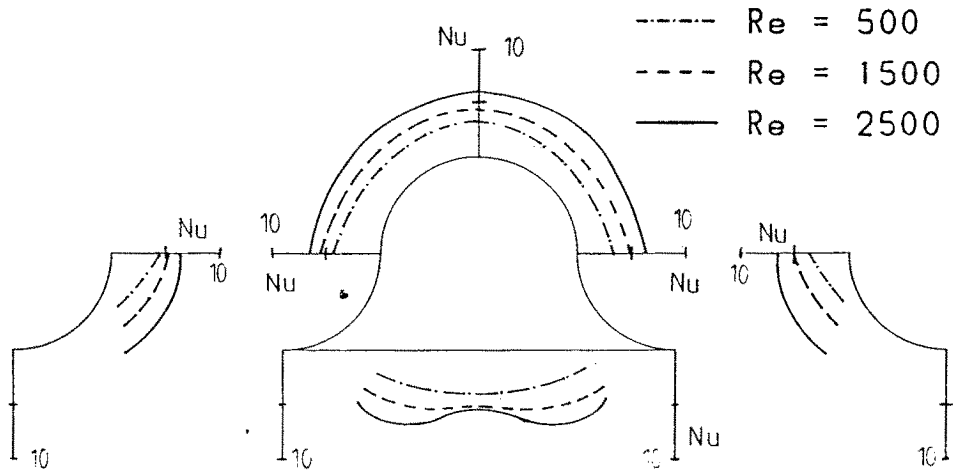

Fig. 6 Local distribution of Nusselt number for square ducts with corner radii of 5 mm

The duct with a corner radius of 1 mm leads to the maximum Nusselt numbers, whereas the lowest Nusselt numbers were measured for the test matrix with radii of 5 mm. The Nusselt number for the geometry with 1 mm radii is about 15 % higher than that for the duct with a radius of 5 mm.

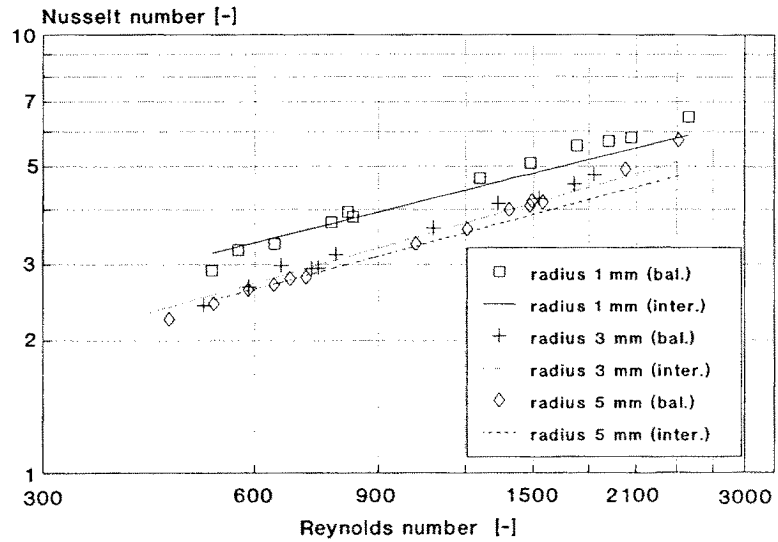

Fig. 7 Nusselt number as a function of Reynolds number for plain fin arrangements

The Nusselt number behaviour is linear as shown in Fig. 7. For this reason a relationship

$$Nu = cRe^{b}\left(\frac{d_{hyd}}{l}\right)^{1/2} \tag{2}$$

describing the total Nusselt number as a function of the Reynolds number, was calculated by means of least square methods. The exponent b in Eq. (2) was assumed to be equal for all geometries because of the parallel straight lines in Fig. 7. The influence of entrance effects was considered by the factor d_{hyd}/l in Eq. (2) depending on the hydraulic diameter and the test matrix length. The exponent 0.5 was chosen according to Pohlhausen [6] . For different geometries the following correlations were derived:

$$\begin{aligned} r = 1 \qquad & Nu = 1.464Re^{0.4}\left(\frac{d_{hyd}}{l}\right)^{0.5} \\ r = 3 \qquad & Nu = 1.301Re^{0.4}\left(\frac{d_{hyd}}{l}\right)^{0.5} \\ r = 5 \qquad & Nu = 1.283Re^{0.4}\left(\frac{d_{hyd}}{l}\right)^{0.5} \end{aligned} \tag{3}$$

The difference between measured and calculated (Eq. (3)) Nusselt number is less than 4%.

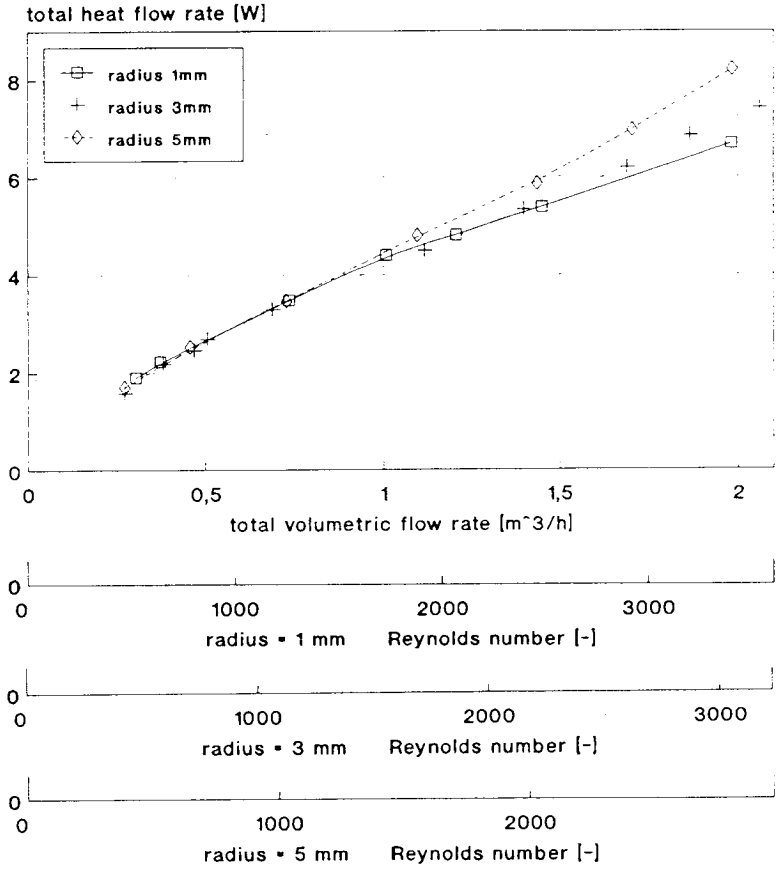

Fig. 8 Total heat flow rate dependent on total volumetric flow rate

Sometimes the total heat flow rate is of interest as function of the total volumetric flow rate of a heat exchanger. The corresponding diagram is shown in Fig. 8 for one duct investigated within this paper. For laminar flow no clear difference between the three test matrices can be seen. For the Reynolds number range greater than 1500 the duct with corner radii of 5 mm shows the best heat transfer characteristic contrary to Fig. 7. A transition regime form laminar to turbulent flow was observed for Reynolds numbers between 1.500 and 2.000. The heat transfer surface is maximum and the hydraulic diameter is minimum for this matrix resulting in an optimum of the total heat flow rate. In the transition region the enhancement of the total heat flow rate is 25 % using corner radii of 5 mm compared to radii of 1 mm and 15 % compared to radii of 3 mm.

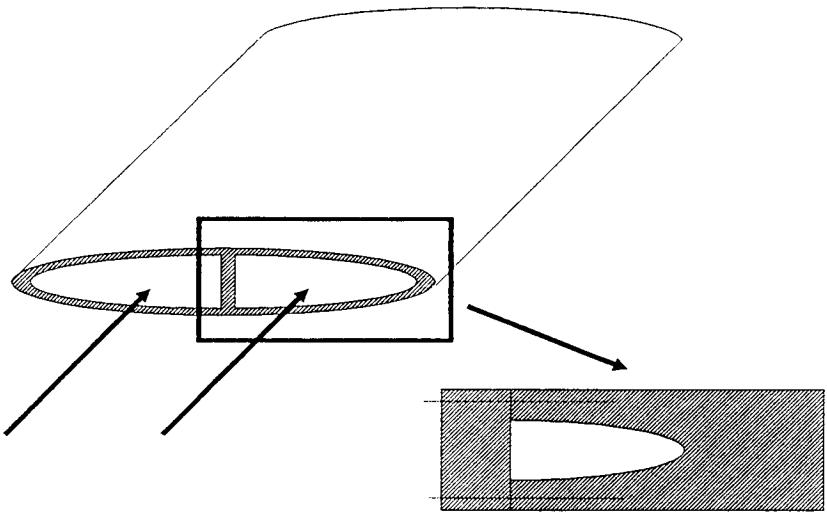

Fig. 9 Flow in a semi-oval duct

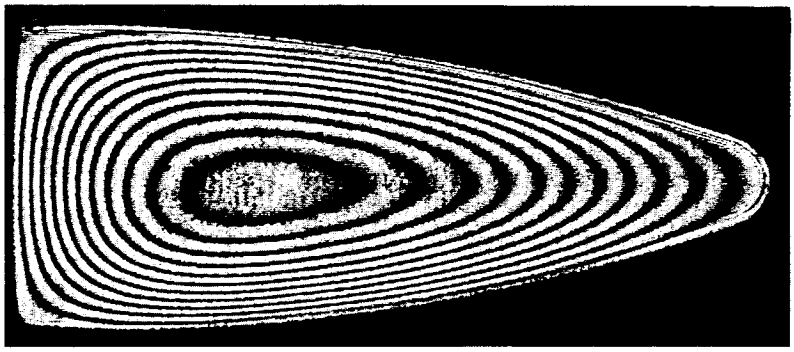

Fig. 10 Interferogram of a semi-oval shaped duct (Re = 800)

5. FLOW IN A SEMI-OVAL DUCT

Sometimes shell and tube heat exchangers with special shaped oval tubes are used for intercoolers and exhaust gas recuperators. The cross section of the tube consists of two symmetrical sections, divided by a parting wall illustrated in Fig. 9. In order to calculate the temperature distribution of the tube with high accuracy the exact knowledge of local heat transfer coefficients is necessary. In addition regions with low heat transfer can be detected and improved. Here the internal flow through one of these semi-oval ducts is investigated. An interferogram describing the temperature distribution at a Reynolds number of 800 is given in Fig. 10. Since the length of the test matrix and the thermal boundary conditions are the same as in the preceding experiments, the temperature difference between two adjacent isotherms is 2.3 K as well. The hydraulic diameter d_{hyd} is calculated by Eq. (1).

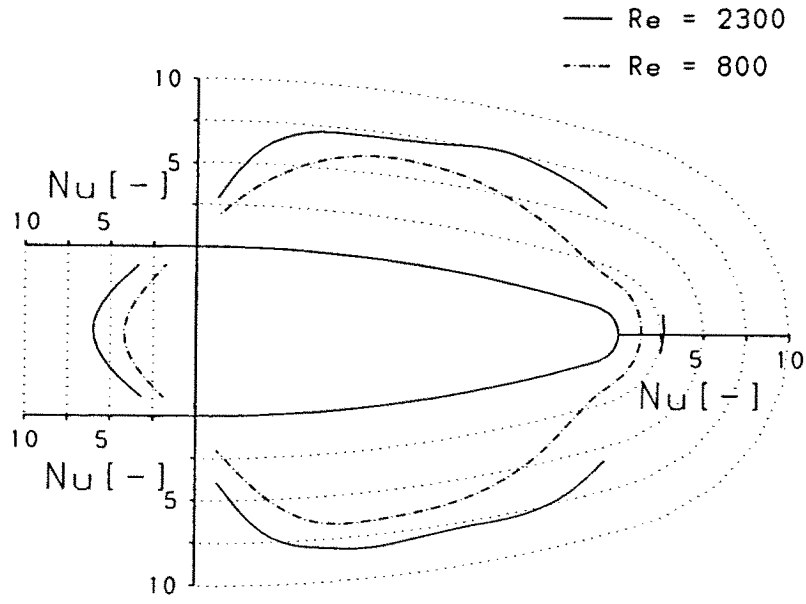

Fig. 11 Distribution of the local Nusselt number in a semi oval shaped duct

In Fig. 11 the Nusselt number distribution for a laminar (Re = 800) and a turbulent (Re = 2300) flow is illustrated. The maximum heat transfer coefficients are located in the middle of each side, whereas the heat flux decreases near to the corners as a result of the low flow velocity at this part of the cross-section. In this region the heat transfer reaches only 30 % of the average heat transfer for low Reynolds numbers and about 50 % at the transition to turbulent flow. The best heat flux occurs along the weakly shaped surface at about half distance between the corners. For laminar flow the heat transfer at the upper side is higher than at the lower one as a result of the overlaid natural convection. The turbulent flow near to the wall is not as slow as in the laminar flow regime resulting in a wider region with better heat transfer.

6. CIRCULAR SEGMENT SHAPED TURBULENCE PROMOTORS

Turbulence promotors often lead to a considerable enhancement of the heat transfer. Rectangular shaped obstacles cause relatively high pressure losses with flow separations at the rib. In order to avoid sharp edges ribs can be shaped circular. To study the influence of circular segment shaped ribs, two test matrices were manufactured and fixed together forming the rectangular duct illustrated in Fig. 12. Therefore the test duct consists of two wider, ribbed sides and two small plain spacers made of glass. Due to aspect ratio of the test section (duct height d : duct width b = 1 cm : 15 cm) an almost two-dimensional flow patterncan be assumed. Rotating one plate staggered and non-staggered fin arrangements were investigated. Additionally a test section was performed with ribs inclined by an angle of 20° to the flow with opposite orientation

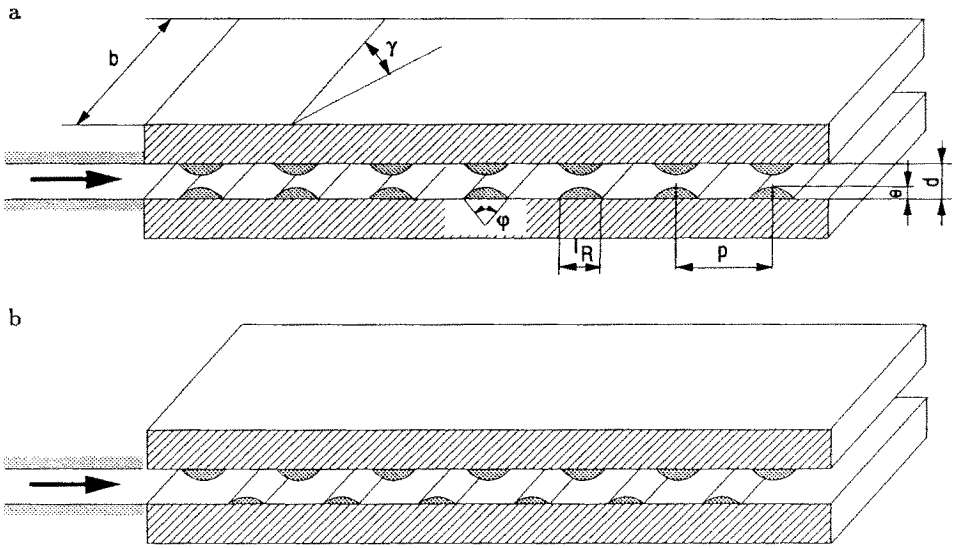

Fig. 12 Non-staggered (a) and staggered (b) arrangements of investigated turbulence promotors

Table 2 Dimensions of plain fin arrangements

		matrix a	matrix b
height of duct	d	10 mm	10 mm
width of duct	b	150 mm	1500 mm
height of ribs	e	3 mm	3 mm
length of ribs	l_r	10 mm	10mm
circular segment angle	φ	120°	120°
rib spacing	p	30 mm	30 mm
angle of attack	γ	0°	20°
arrangements		staggered non-staggered	inclined

of the ribs on the two walls leading to a crossed-rib arrangement. Rib dimensions and rib pitch were held constant during the experiments. According to parallel plates the hydraulic diameter d_{hyd} is defined:

$$d_{hyd} = 2d \tag{4}$$

Characteristic data are given in Table 2. Figure 13 shows interferograms for different

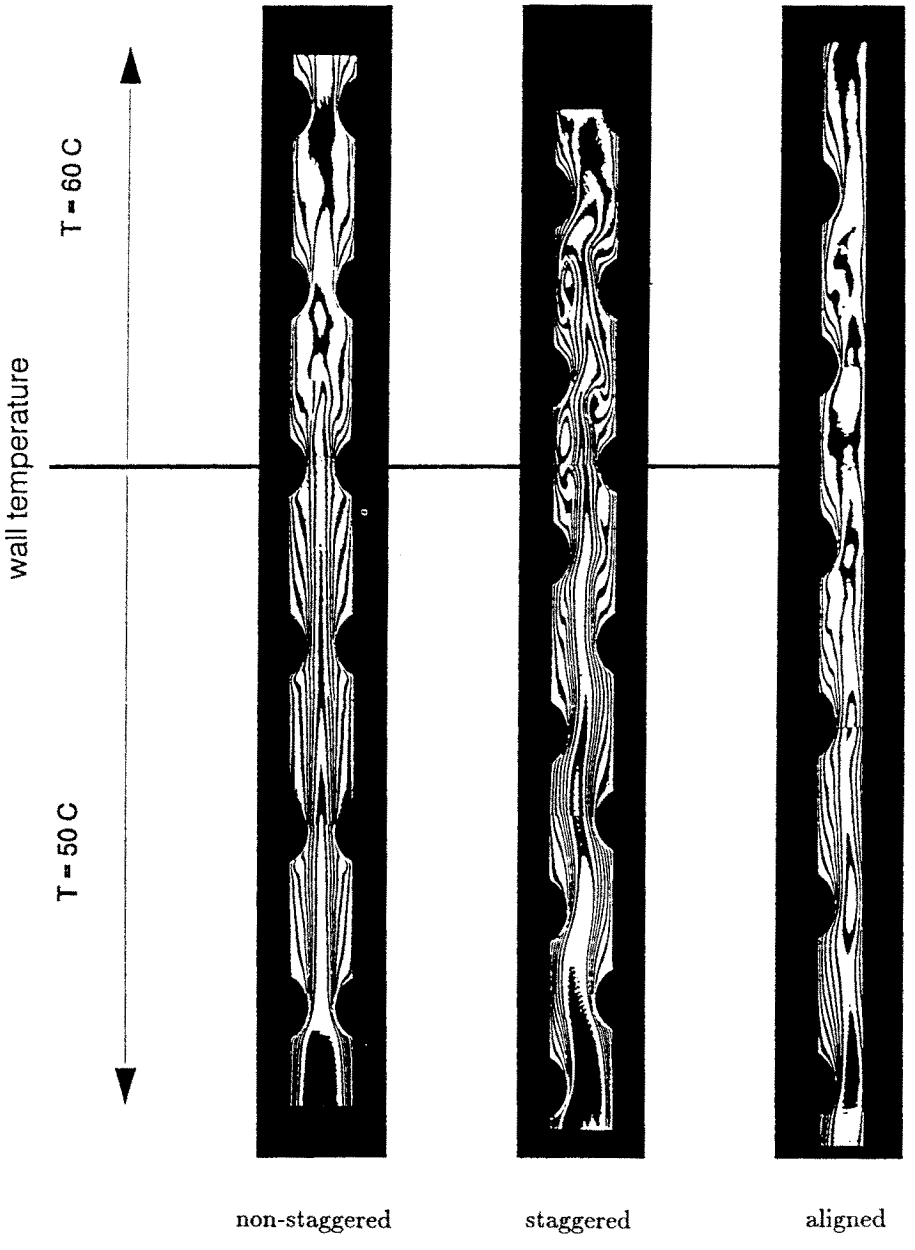

Fig. 13 Interferograms of circular segment shaped ribs (Re = 1500)

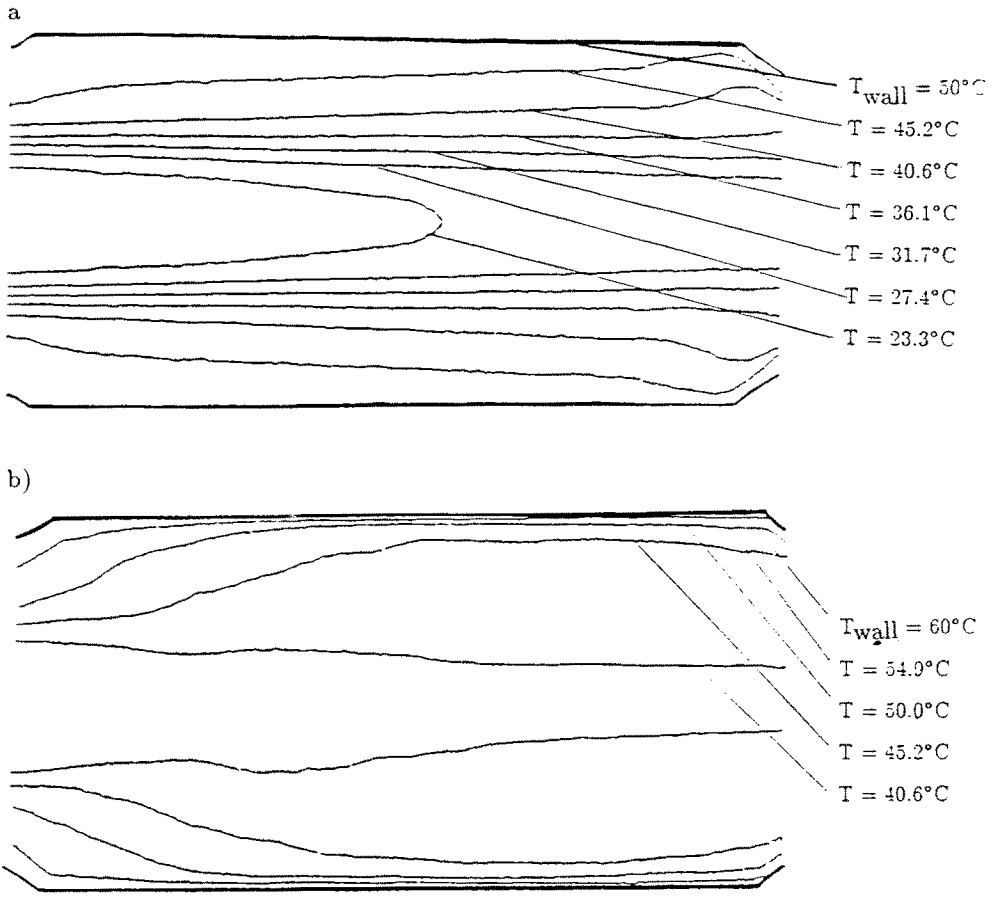

Fig. 14 Temperature profiles in the wake of the first (a) and the fifth (b) obstacle (non-staggered arangement)

arrangements taken at a Reynolds number of 1500. At this condition the effect of the ribs as turbulence promotor are ascertained. Whereas the flow is laminar in the entrance region of the duct, it changes to turbulent between the third and fifth obstacle resulting in a highly increased Reynolds number. This effect is elucidated by Fig. 14 where the temperature profiles are shown for the wake of the first and the fifth obstacle. In Fig. 14a the largest temperature drop occurs in the centre of the duct, whereas the temperature gradient is noticeable high close to the wall for turbulent flow. For the latter a relatively low temperature gradient in the duct middle wsas found. The inlet effect on the heat transfer is depicted for the staggered arrangement in Fig. 15. The heat transfer in the wake of the first rib relatively low due to the laminar flow condition and increases by 150 % in the wake of the fifth further ribs.

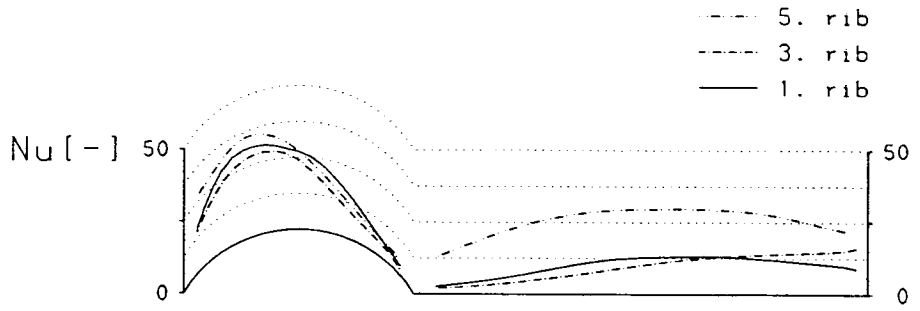

Fig. 15 Entrance effects and heat transfer enhancement for a Reynolds number of 1500 (staggered arrangement)

The local Nusselt number distribution at the fifth obstacle and in the following groove is illustrated in Figs. 16 and 17 describing a fully developed flow. A comparison with the behaviour at the down- and upstream rib validates a fully developed flow with a heat transfer that is no longer dependent on the rib number. The heat transfer along the obstacle is maximum for the non-staggered ribs. The minimum flow cross section between the ribs compared to the other arrangements leads to high local velocities and therefore to increased convective heat fluxes. On the other hand the heat transfer is relatively low for the staggered ribs. In the gap between the obstacles the non-staggered ribs show only very small heat transfer coefficients for laminar flow. The main mass flow was found in the centre of the duct with a widely decreasing convective part of the heat transfer in the wake of the ribs. The Nusselt number reaches only about 15 % of the maximum value immediately after the rib at the obstacle itself and increases slightly to approximately 25 % at the following rib. In this region both other arangements show better heat transfer rates with maximum heat transfer at approximately half the distance between two obstacles.

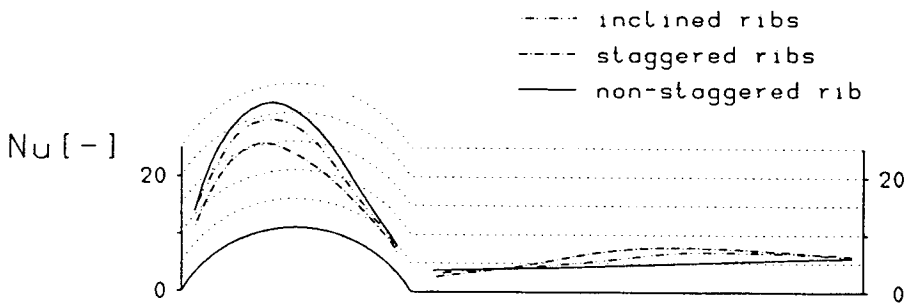

Fig. 16 Local Nusselt number distribution for laminar flow (Re = 500) after the fifth rib

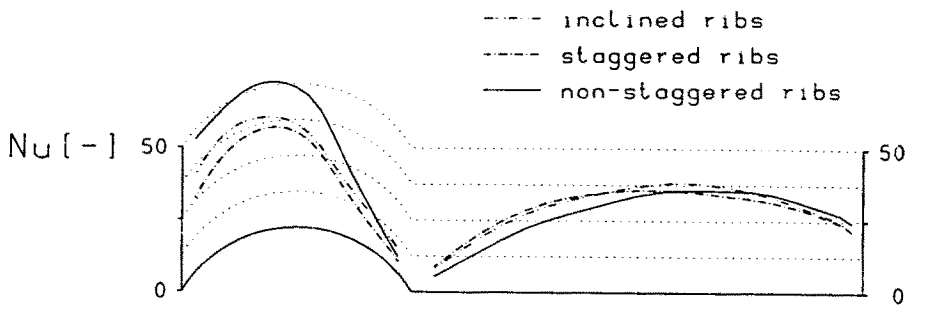

Fig. 17 Local Nusselt number distribution for a turbulent flow (Re = 2500) after the fifth rib

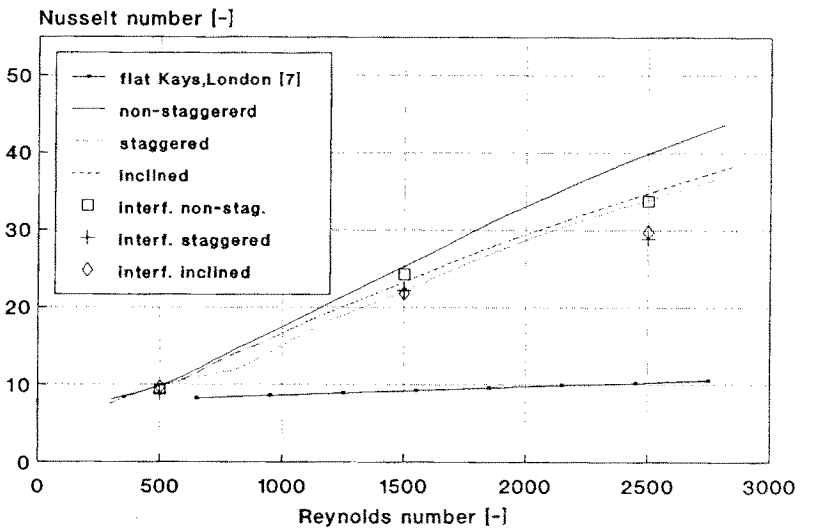

Fig. 18 Nusselt number as a function of Reynolds number for circular segment shaped obstacles

In Fig. 17 the corresponding distribution for turbulent flow (Re = 2500) is illustrated. The Nusselt number shows almost the same behaviour along the obstacle as for laminar flow conditions, but with increased values. Caused by turbulence effects the heat transfer between two obstacles is enhanced to the same level as at the obstacle itself. For all investigated geometries a maximum of heat transfer arises between 1/2 and 2/3 downstream the obstacle. It is obvious that the heat transfer at non-staggered ribs is about 25 % higher than for the two other geometries and falls more than for the other arangements subsequent to the obstacles.

The overall Nusselt number was measured by energy balance methods as well in order to approve the results of the interferometric measurements. It can be seen in Fig. 18 that the non-staggered ribs lead to the best heat transfer. Basicly t he staggered and the inclined arrangements show similar behaviour with slight advantages in heat transfer of the inclined ribs. The interferometric measurements correspond with the caloric results for Reynolds numbers of 500 and 1500 within a range of 5 %. For a Reynolds number of 2500 a difference of 15 % occurs, supposedly due to the thin boundary layer at the obstacles. In Fig. 18 the heat transfer in a flat duct, i.e. between parallel plates, is shown for comparison. It was calculated by equations given by Shah and London [7] . According to this results an enhancement of heat transfer of 100 % for low Reynolds numbers and of approximately 300 % for Reynolds number of 2500 can be achieved.

7. NOMENCLATURE

A	m^2	total heat transfer area
A_c	m^2	flow cross-sectional area
b	m	width of duct
d	m	height of duct
d_{hyd}	m	hydraulic diameter
e	m	rib height
h	$Wm^{-2}K^{-1}$	heat transfer coefficient
k	$Wm^{-2}k^{-1}$	fluid thermal conductivity
l	m	length of the test matrix
l_r	m	fin length, rib length
Nu	–	Nusselt number, $Nu = hd_{hyd}/k$
p	m	rib spacing
$\dot{Q}$	W	heat transfer rate
Re	–	Reynolds number, $Re = \rho w_m d_{hyd}/\mu$
T	K	temperature
t_f	m	fin thickness
ΔT_m	K	logarithmic mean temperature difference
U	$Wm^{-2}k^{-1}$	overall conductance
V	m^3	heat exchanger volume
w_m	m s^{-1}	fluid mean axial velocity
β	m^2/m^3	area density
γ	°	angle of attack
μ	Pa s	fluid dynamic viscosity
φ	°	circular segment angle
ρ	kg m^{-3}	fluid density

ACKNOWLEDGEMENT

Work is supported by the Federal Minister for Research and Technology the Federal Republic of Germany through the Forschungszentrum Jühlich GmbH and assisted by the Motoren u. Turbinen-Union, München.

REFERENCES

[1] Shah, R.K.: Compact and enhanced heat exchangers; in: Taborek, J., Hewitt, G.F., Afgan, N.: Heat Exchangers – Theory and Practice; McGraw-Hill Book Company; (1983);

[2] Shah, R.K.: Classification of Heat exchangers; in Kakac, S., Bergles, A.E., Mayinger, F.: Heat Exchangers – Thermal Hydraulic Fundamentals and Design; McGraw-Hill Book Company; (1981);

[3] Hauf, W., Grigull, U.: Optical Methods in Heat Transfer; Advances in Heat Transfer, Vol. 6(1970), Academic Press, New York;

[4] Chen, Y.M., Mayinger, F.: Holographic interferometry studies of the temperature field near a condensing bubble; in: Optical methods in dynamics of fluids and solids; Proc. of an int. sympos; Sept. 17-21; IUTAM; ed.: M. Pachal; Berlin, (1985);

[5] Mayinger, F., Panknin, W.: Holography in heat and mass Transfer; Proc. of the 5th Int. Heat Transfer Conference, Tokio, Vol. VI, (1974);

[6] Pohlhausen, E.: Der Wärmeaustausch zwischen festen Körpern und Flüssigkeiten mit kleiner Reibung und Wärmeleitung; Angew. Math. Mech. 1(1921);

[7] Shah, R.K., London, A.L.: Laminar Flow Forced Convection in Ducts; Supplement 1 to Advances in Heat Transfer, Academic, New York, (1978);